Capacity configuration method of flexible smart traction power supply system based on double-layer optimization

Yichen Ying, *Graduate Student Member, IEEE*, Zhongbei Tian, *Member, IEEE*, Mingli Wu, *Member, IEEE*, Qiujiang Liu, *Member, IEEE*, and Pietro Tricoli, *Member, IEEE*

***Abstract*—The flexible smart traction power supply system (FSTPSS) is a new type of traction power supply system including converters, energy storage devices and renewable energies. The capacities of the multiple components in FSTPSS have a significant impact on the economic operation and stable operation. And the capacity configuration optimization requires to consider both the daily operation costs and long-term investment recycle, which has not been fully studied. Based on the characteristics of FSTPSS, this paper proposes a double-layered capacity configuration optimization method by integrating artificial fish swarm algorithm and CPLEX solver. The main goal of this method is to obtain the maximum economic benefits in the whole life cycle. Meanwhile, the operation time of FSTPSS when facing grid outage is also considered. The simulation results show that compared with benchmark, the final converged maximum benefit value has increased by 43.6%, the grid power is averaged cut by 2.26%, the sum of daily cycle number of the energy storage devices increased by 27.3%. In addition, the proposed method can also improve the probability that train can drive out of the current power supply interval in the event of grid outage. By using the proposed method, this probability is increased by 9.27%.**

Index Terms—**capacity configuration; operation time during grid outage; traction power supply system; energy storage devices; renewable energy; converter**

I. Introduction

NOWADAY, the distributed energy sources such as PV generation and wind power generation are increasing dramatically. They are widely distributed across the country. Traction power supply system (TPSS), as a system that is also spread all over the country, has a huge potential for accessing distributed energy sources and absorbing it in real time. FSTPSS is such a new TPSS that considers distributed power sources and energy storage devices. The concept of FSTPSS was first proposed in [1] which is a fully electronic TPSS with smart energy management strategy, before that, there was a similar concept called the flexible

This research was supported by the Fundamental Research Funds for the Central Universities (Science and technology leading talent team project) (2022JBQY008). (*Corresponding author: Mingli Wu, Zhongbei Tian*)

Yichen Ying, Qiujiang Liu, and Mingli Wu are with the School of Electrical Engineering, Beijing Jiaotong University, Beijing 100044, China (e-mail: ycying@bjtu.edu.cn; qjliu@bjtu.edu.cn; mlwu@bjtu.edu.cn).

Zhongbei Tian is with the Department of Electrical Engineering and Electronics, University of Liverpool, Liverpool L69 3BX, UK (e-mail: zhongbei.tian@liverpool.ac.uk).

Pietro Tricoli is with the Department of Electronic, Electrical and Systems Engineering, University of Birmingham, Birmingham B15 2TT, U.K. (e-mail: p.tricoli@bham.ac.uk).

traction power supply system (FTPSS), which can be found in [2,3]. In [1], a day-ahead energy management of FSTPSS based on fixed capacity configuration have been fully studied. However, at present, the problem of how these fixed capacity configurations are determined has not been solved. Therefore, this paper aims to propose a capacity configuration optimization method specifically for FSTPSS.

At present, in terms of power system, there are some capacity configuration optimization methods that can be used for reference. Wang *et al.* [4] presented a capacity configuration optimization method for microgrid energy storage devices based on PV, energy storage devices, and noncritical loads. However, the proposed method only considers the maximum energy demand of the energy storage device, and the economy of the energy storage device capacity has further room for optimization. Soltani *et al.* [5] developed an optimal capacity allocation method for energy storage devices and renewable energy considering the uncertainty of load and renewable energy. By adding the uncertainty of load and renewable energy as chance constraints to the optimization problem, the result obtained the optimal capacity configuration that can be accepted in practical situations. Petrelli *et al.* [6] proposed a capacity configuration optimization method for microgrids in remote areas considering the battery degradation model. The battery degradation model was used to calculate the precise life cycle of the battery, thereby deriving the expected revenue of the battery in the full life cycle. This method is more accurate in estimating the expected benefits of the battery, but due to the addition of the battery degradation model, its calculation time is longer. The energy storage device model used above all have the problem to calculate the large-scale energy storage system in a suitable time. For large-scale energy storage system, a simple but efficient energy storage device model is usually used, and some more intelligent optimization methods are used to reduce the optimization time. In [7], a game theoretic-related optimization method for the capacity configuration of microgrids was proposed. Since multiple devices are included for joint optimization, the models used are almost all linear models which could effectively reduce the computation time. Using multiple time scales is also a common way to reduce computation time, in [8] a capacity configuration method for energy storage devices that considers multiple time scales was proposed. And both the computation time and the result accuracy of co-optimization of multiple time scales is acceptable. These paper shows that we can use an approximate energy storage device model to reduce the calculation time without too much impact on our calculation results that meet the requirements.

The above research fully considers the influence of the load characteristics of the microgrid itself on the capacity selection of energy storage devices, but they neglect the system flexibility which could deal with potential system power shortage risks. In fact, there are some studies pointed out that add additional constraints could make the final optimization results have flexibility. Madathil *et al.* [9] proposed a microgrid capacity configuration optimization method considering the resilience of the microgridby adding N-1 security constraints to the optimization model. Thompson *et al.* [10] analyzed the relationship between the capacity of microgrid energy storage devices of microgrid and the economics of the microgrid. And the conclusion is that the profit of the

microgrid is the highest when the gap between the discharge revenue and the charging loss of the energy storage device is the largest. Arefifar *et al.* [11] developed a capacity configuration and location method for microgrid distributed reactive power and distributed energy storage devices considering reliability. The optimization results show this method can improve the overall reliability of the system. In [12], a double-layer configuration optimization method was proposed. The optimization of the first layer determines whether corresponding configuration components should appear. The capacity configuration of the second layer is to configure the capacity of the corresponding configuration component size. In [13], an optimization method for energy storage configuration of multi-energy systems considering system flexibility was proposed. The flexibility index is defined as the sum of the reduction rates of the final load, and the flexibility index is added to the optimization as a constraint condition. Considering that the microgrid may operate in an islanded operation state, Lee *et al.* [14] presented a method to determine the optimal reserved capacity of the microgrid based on the power exchange for frequency control market environment, which can make the microgrid have enough energy storage capacity to cope with the power supply problems in island mode. The above paper proves that the reliability of the power system could be improved by using a proper method.

Yet, the method mentioned above only considers the conventional load in the power system, which cannot directly used in TPSS. In fact, for TPSS, there is also some research on the optimization method of capacity configuration. In [15], a capacity configuration optimization method of TPSS based on supercapacitor energy storage is proposed. The optimization objective considered regenerative braking energy, negative sequence power and economic benefits. The method proposed in this article is more practical, but the efficiency of the optimization method used is too low. Luo *et al.* [16] proposed a capacity configuration optimization method for railway static power conditioner with energy storage system in TPSS. The optimization goal of this optimization method is to obtain an energy storage capacity configuration that enables the system to have optimal economic performance and its adjusted variable is the charge and discharge threshold of the energy storage device. Darco *et al.* [17] proposed a PV capacity configuration method for a hybrid PV TPSS. The relevant numerical simulation experiments prove that in a hybrid PV TPSS, a large number of PV power plants should be installed to offset the installation cost of power electronic devices. Zhu *et al.* [18] proposed a two-stage energy storage system parameter optimization method. The optimization goal of the upper layer is to improve the regenerative energy recovery rate of the energy storage system, and the lower layer is to optimize operating energy consumption. But this method does not consider the long-term investment recycle. Zahedmanesh *et al.* [19] proposed a capacity configuration optimization method for the TPSS including PV and energy storage systems. The method is divided into two parts, the first part is the sequential decision-making process which could make the system meet the requirements of demand power and power quality, and the second part is the capacity optimization of converters of PV and battery, which could reduce the system unbalance and provide sufficient reactive power compensation capacity. Yet, none of the capacity configuration optimization method used in TPSS has considered the daily operation costs and long-term investment recycle problem at the same time, especially for the

scenarios based on FSTPSS. The above optimization methods have certain reference significance for the capacity configuration optimization of FSTPSS. But since FSTPSS is a brand-new TPSS topology, these methods cannot be directly applied to FSTPSS.

In order to build a capacity configuration optimization method for FSTPSS, the first thing we need to do is to find a suitable optimization algorithm. In terms of optimization algorithms, we generally refer to the optimization algorithm of route optimization, since it is more intuitive and more explanatory. In [20], an optimization method for trajectory planning of unmanned vehicles based on artificial fish swarm algorithm (AFSA) and trial-and-error search algorithm was proposed. The results of the operation show that AFSA has the powerful optimization computing ability and has the ability to find the global optimal solution better than the genetic algorithm, particle swarm algorithm and other evolutionary algorithms. Tang *et al.* [21] compared the advantages and disadvantages of some modern swarm intelligence algorithms. Among them, for AFSA, they pointed out that it had the advantages of faster convergence speed, stronger global search ability and required fewer parameters to adjust. Lei *et al.* [22] used AFSA to identify essential proteins, which has better results than traditional identification algorithms.

In fact, AFSA can also be used in the problem of capacity configuration optimization, because the capacity configuration optimization problem, to some certain extent, can also be understood as a trajectory problem, we need to find a set of optimal trajectories (capacity configuration), which makes our time optimal (target optimal). Therefore, this paper chooses to use AFSA as the upper layer optimization method for our capacity configuration optimization.

Based on the above analysis, this paper proposes a capacity configuration optimization method for FSTPSS, and uses the scenario based on measured data to verify the feasibility of the method. The main contributions of this paper are as follows:

1). Aiming at the capacity configuration problem of FSTPSS, a capacity configuration method for FSTPSS based on double-layer optimization is proposed. To the best of our knowledge, this is the first capacity configuration method for FSTPSS. CPLEX solver is used to solve the maximum daily profit of FSTPSS under specific parameters, and AFSA is used to determine specific parameters, which ensure that the FSTPSS has the maximum benefit during its life cycle.

2). In order to make the train pass through the power supply section reliably when the grid outage happens, reliability constraints are added in the capacity configuration method, so that the configured parameters can not only meet the requirements of economy, but also meet the requirements of reliability.

3). The proposed method is verified by a real case study. The simulation results prove that compared with the traditional TPSS, a FSTPSS with good capacity configuration parameters can have better economy and reliability. In addition, compared with the FSTPSS using the benchmark parameters, the FSTPSS using the parameters configured by the capacity configuration method proposed in this paper has the better economy, capacity utilization, reliability and can reduce the energy it obtains from the power grid.

The rest of this paper is arranged as follows: Section II introduces the topology and energy constraints of FSTPSS. Section III

describes the capacity configuration method of this paper. Section IV is the case study and Section V gives the conclusion.

II. System Description

A. System Topology

The topology of FSTPSS is shown in Fig. 1. FSTPSS consists of AC-DC-AC traction substation, traction network and wayside microgrid. Their respective functions are as follows:

The AC-DC-AC traction substation could achieve symmetrical power supply and eliminate harmonics of traction load. UC (ultra-capacitor) and battery are connected to the DC side of AC-DC-AC traction substation to recover the regenerative braking energy and excess PV power and to realize the function of peak shaving and valley filling. Since the battery has a large energy density, the battery is actually be regarded as the main energy recovery device.

The traction network is the main transmission path for the traction load to obtain power. The wayside microgrid is mainly used to connect the distributed generation along the railway line and the 10kV distribution network. The excess power of the wayside microgrid could be sold to 10kV distribution network. UC is also added to the DC bus on the wayside microgrid side so that the wayside microgrid can also output its power more smoothly.

B. Network Power Balance

For FSTPSS, the most basic constraint is its power balance constraint. FSTPSS shown in Fig. 1 can be divided into two parts: part 1 is the main traction power supply network from high voltage power grid, and part 2 is the 10kV distribution network. The power balance constraints of these two parts can be expressed by (1-2):

$$\begin{aligned} &P_{sub-grid}^{t} + P_{sub,bat,dis}^{t} + P_{sub,uc,dis}^{t} + P_{PV}^{t} + P_{DC,uc,dis}^{t} = \\ &P_{sub,bat,ch}^{t} + P_{sub,uc,ch}^{t} + P_{DC,uc,ch}^{t} + P_{T}^{t} + P_{DC-load}^{t} + P_{sub-grid,fed}^{t} \quad \forall t \end{aligned} \tag{1}$$

$$P_{DC\text{-}load}^{t} + P_{10kV\ grid}^{t} = P_{10kV\ load}^{t} \tag{2}$$

where $P_{sub\text{-}grid}^{t}$ is the positive power of 220kV power grid. $P_{sub\text{-}grid,fed}^{t}$ is the negative power of 220kV power grid. $P_{10kV\,grid}^{t}$ is the power of 10kV power grid. $P_{sub,bat,dis}^{t}$, $P_{sub,bat,ch}^{t}$, $P_{sub,uc,dis}^{t}$ and $P_{sub,uc,ch}^{t}$ are discharging and charging power of Battery and UC on the DC side of AC-DC-AC traction substation, respectively. $P_{DC,uc,dis}^{t}$ and $P_{DC,uc,ch}^{t}$ are discharging and charging power of UC on the DC side of wayside microgrid. $P_{DC\text{-}load}^{t}$ means the power provided by the microgrid to the 10kV distribution network. P_{PV}^{t}, P_{T}^{t} and $P_{10kV\,load}^{t}$ are respectively denotes the predicted power of PV panel, traction load and 10kV distribution network load.

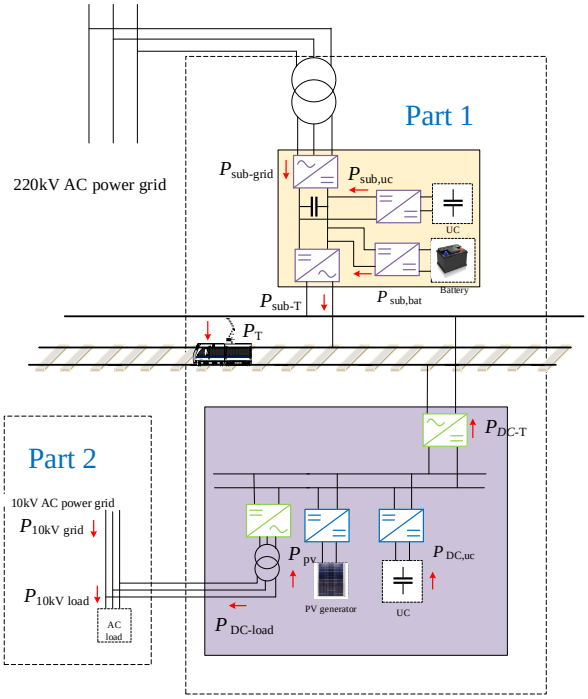

Fig. 1. Topology of FSTPSS.

C. Constraints of Energy Storage Devices

For energy storage devices such as battery and UC, their power is limited by their own residual energy and rated power, so they have constraints as shown in (3-5):

$$E_i^t = (1-\kappa_i)E_i^{t-1} + \eta_i^{ch} P_{i,ch}^t \Delta t - P_{i,dis}^t \Delta t / \eta_i^{dis} \quad \forall i,t \tag{3}$$

$$0 \le P_{i,ch}^t \le \min(P_i^{rated}, (E_i^{rated} \cdot SOC_i^{\max} - E_i^{t-1}) / (\eta_i^{ch} \cdot \Delta t)) \quad \forall i,t \tag{4}$$

$$0 \le P_{i,dis}^t \le \min(P_i^{rated}, (E_i^{t-1} - E_i^{rated} \cdot SOC_i^{\min}) \cdot \eta_i^{dis} / \Delta t)) \quad \forall i,t \tag{5}$$

where i means the energy storage device i. It could be battery or UC. E_i^t presents its residual energy. E_i^{rated} denotes its rated energy capacity. η_i^{dis} and η_i^{ch} are discharging efficiency and charging efficiency of it, respectively. κ_i is its self-discharging rate. $P_{i,dis}^t$ and $P_{i,ch}^t$ are discharging and charging power of it. P_i^{rated} denotes its rated power. SOC_i^{max} and SOC_i^{min} are respectively represent its maximum and minimum value of state of charge. Δt represents the calculation interval of algorithm.

In order to make the energy storage device operate under the same initial state every day, additional energy constraints are added as shown in (6):

$$E_i^{t=1} = E_i^{t=end} \quad \forall i \tag{6}$$

In addition, the capacity of the energy storage device should be larger than the maximum energy demand when passing through the power supply interval, as it is necessary to consider the reliable operation of the train out of the current power sup-ply interval in case of power failure of the grid, which function is similar to uninterruptible power supply (UPS). Therefore, the constraints shown in (7) need to be added.

$$\sum_{i=1}^{N} (E_i^{current} - E_i^{\min}) \ge \sum_{t=1}^{\tau} P_{\max load}^t \cdot \Delta t \tag{7}$$

where $E_i^{current}$ is the remaining energy of the energy storage device i in the current state, and N is the total number of energy storage

devices. E_i^{min} is the minimum energy limit of the energy storage device i. $P_{max\ load}{}^t$ represents the power of the t_{th} time step in the traction load power sequence. τ denotes number of the time step required for the train to pass through the power supply interval.

D. Limitations from PV Panels and Converters

The power flow in FSTPSS should also be limited by the rated power of the converters which connect the various parts, as shown in (8-12):

$$P_{sub-grid}^t \le P_{sub,conv}^{3PH} \quad \forall t \tag{8}$$

$$P_{sub-grid,fed}^t \le P_{sub,conv}^{3PH} \quad \forall t \tag{9}$$

$$P_{sub-grid}^t + P_{sub,uc,dis}^t + P_{sub,bat,dis}^t \le P_{sub,conv}^{1PH} \quad \forall t \tag{10}$$

$$P_{PV}^t + P_{DC,uc,dis}^t - P_{DC-load}^t \le P_{DC,conv} \quad \forall t \tag{11}$$

$$0 \le P_{DC-load}^t \le P_{DC-load,conv} \quad \forall t \tag{12}$$

Among them, $P_{sub,conv}{}^{3PH}$ and $P_{sub,conv}{}^{1PH}$ present the rated power of three-phase and single-phase converter of the AC-DC-AC traction substation, respectively. $P_{DC,conv}$ indicates the rated power of converter which connects the wayside microgrid and traction network. $P_{DC\text{-}load,conv}$ denotes the rated power of converter connecting the wayside microgrid and 10kV distribution network.

For the output power of PV panel, it should be limited by rated output power of PV panel, as shown in (13):

$$0 \le P_{PV}^t \le P_{PV}^{rated} \quad \forall t \tag{13}$$

where $P_{PV}{}^{rated}$ presents the rated output power of PV.

E. Short-circuit Capacity Constraints

Finally, the power of the grid is also limited by its own short-circuit capacity, as shown in (14-16):

$$0 \le P_{sub\text{-}grid}^t \le S_{220kV\ grid}^{short} \quad \forall t \tag{14}$$

$$0 \le P_{sub\text{-}grid,fed}^t \le S_{220kV\ grid}^{short} \quad \forall t \tag{15}$$

$$0 \le P_{10kV\ grid}^t \le S_{10kV\ grid}^{short} \quad \forall t \tag{16}$$

where $S_{220\ kV\ grid}{}^{short}$ and $S_{10kV\ grid}{}^{short}$ are short-circuit capacity of 220kV power grid and 10kV power grid respectively.

III. DOUBLE-LAYERED CAPACITY CONFIGURATION METHOD

A. Double-layer optimization scheme

The schematic diagram of the double-layer optimization is shown in Fig. 2.

As can be seen from the figure, the optimization goal of the upper layer is mainly to obtain the optimal capacity configuration, and its input is the daily energy management strategy (DEMS) of FSTPSS and the daily revenue obtained by DEMS. Since the upper layer optimization is a nonlinear optimization problem, it is implemented by AFSA that specializes in solving nonlinear optimization problems.

The optimization goal of the lower layer is to obtain the optimal DEMS. Its input is the operation scenario and capacity

parameters. The lower layer optimization is a mixed integer linear programming (MILP) problem, so it is implemented by the CPLEX solver developed by IBM that can solve MILP problems [23-25]. The solver uses branch-and-cut method to solve MILP problems.

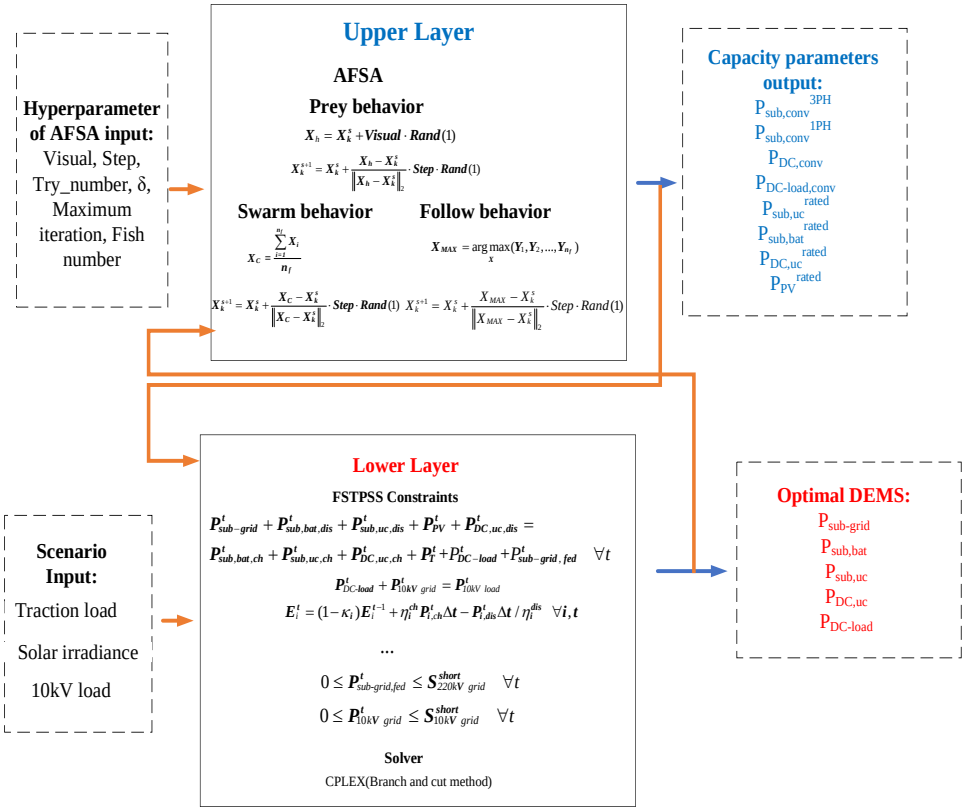

Fig. 2. Schematic diagram of double-layer optimization

B. Capacity Configuration Method

The initial investment of FSTPSS is mainly divided into four parts, isolation transformers, converters, PV panels and energy storage devices. The investment cost can be calculated by (17):

$$\begin{aligned} C_{invest} = & C_{Tran} + C_{Con} + C_{PV} + C_{ESD} = \lambda_{Tran} \cdot P_{Tran} + \\ & \lambda_{con} \cdot (P_{sub,conv}^{3PH} + P_{sub,conv}^{1PH} + P_{DC,conv} + P_{DC-load,conv}) \\ & + \lambda_{PV} \cdot P_{PV} + \lambda_{uc} \cdot (P_{sub,uc}^{rated} + P_{DC,uc}^{rated}) + \lambda_{bat} \cdot P_{sub,bat}^{rated} \end{aligned} \tag{17}$$

where λ_{Tran}, λ_{con}, λ_{PV}, λ_{uc} and λ_{bat} (¥/MW) present the unit investment cost of isolation transformer, converter, PV panel, UC and battery, respectively. C_{Tran}, C_{con}, C_{PV} and C_{ESD} denotes the investment cost of isolation transformers, converters, PV panels and energy storage devices, respectively.

For an energy storage device, in addition to the parameter of rated power, there should be a parameter of rated capacity. However, for a specific modular energy storage device, the rated power of the energy storage device has a fixed ratio to the rated capacity. Therefore, once the rated power of energy storage device is determined, its rated capacity is also determined.

In the similar way, for PV panels, in addition to the parameter of rated power, there should also be a parameter of PV panel area. For a specific modular PV panel, the area of PV panel also has a fixed ratio to the rated power. So, once its rated power is

determined, its PV panel area is also determined. The formula for calculating the output power of the PV panel can be shown in (18):

$$P_{PV}^{t} = \eta_{PV} \cdot A_{PV} \cdot I_{solar}^{t} \quad \forall t \tag{18}$$

where η_{pv} present the photoelectric conversion efficiency. A_{PV} (m^2) is the PV panel area. $I_{solar}{}^{t}$ (MW/m^2) denotes the solar irradiance.

Since we want to get the capacity configuration that can get the maximum revenue, we can design our objective function according to (19):

$$\max \ R_{total} = 365 \cdot L_{expec}(C_{origin} - C_{optim}) - C_{invest} \tag{19}$$

Among them, L_{expec} is the shortest life expectancy among the various parts of the FSTPSS. C_{origin} means the daily cost of the system before the implementation of DEMS. C_{optim} presents the daily cost of FSTPSS after the implementation of DEMS.

C. Daily Energy Management Strategy

For FSTPSS, its daily cost is mainly composed of two parts, one is the electricity charge, and another is the demand charge. The electricity charge is related to the power obtained by the FSTPSS from the power grid, which can be calculated by the formula shown in (20):

$$C_{EC} = \sum_{t=1}^{T} \pi_{EC}^{t} \cdot P_{sub-grid}^{t} \cdot \Delta t \tag{20}$$

where T is the total number of time step in a day, t is current time step, $\pi_{EC}{}^{t}$ (¥/MWh) denotes the unit price of electricity. Δt (5 mins) presents time step length.

The demand charge is a penalty charge, which is implemented to punish excessive peak power. Its specific calculation formula is shown in (21):

$$C_{DC} = \pi_{DC} \cdot \max(P_{avg}^{1}, P_{avg}^{2}, ..., P_{avg}^{T/3}) \tag{21}$$

where $P_{avg}{}^{t}$ means the average power within 15 minutes of traction substation. $\pi_{DC}{}^{t}$ (¥/MW) denotes the unit demand charge price.

In addition to cost, since the 10kV distribution network is connected to wayside microgrid, FSTPSS can sell a certain amount of electricity to the 10kV distribution network to obtain a certain profit by signing a relevant agreement with the 10kV distribution network. The calculation formula of the revenue can be calculated according to (22):

$$R_{sell} = \sum_{t=1}^{T} (\pi_{EC}^{t} - \pi_{trans}^{t}) \cdot P_{micro-load}^{t} \cdot \Delta t \tag{22}$$

where $\pi_{trans}{}^{t}$ (¥/MW) presents unit power transmission cost.

Based on the above analysis, for DEMS, its objective function can be expressed by (23):

$$\min \ C_{total} = C_{EC} + C_{DC} - R_{sell} \tag{23}$$

In fact, there are some variables in equations (1-2) that cannot appear at the same time, such as UC and battery cannot be charged and discharged at the same time. This problem can be solved by using a binary variable constraint.

D. Algorithm Formulation

For the upper layer optimization, it is implemented by AFSA, and its specific algorithm design is as follows:

In AFSA, artificial fish have four behaviors: prey behavior, swarm behavior, follow behavior, and random behavior. Prey behavior can be defined by (24-25):

$$X_h = X_k^s + Visual \cdot Rand(1) \tag{24}$$

$$X_k^{s+1} = X_k^s + \frac{X_h - X_k^s}{\left\| X_h - X_k^s \right\|_2} \cdot Step \cdot Rand(1) \tag{25}$$

where X_k^s is the current position of artificial fish *k*. X_k^{s+1} is the next step's position of artificial fish *k*. *Visua*l the artificial vision's field. X_h is a random position within the field of vision of artificial fish *i*. Rand(1) means a uniformly distributed random number between -1 and 1. *Step* represents the step size.

For the problem in this paper, the composition of *X* can be defined by (26):

$$X = (P_{sub,conv}^{3PH}, P_{sub,conv}^{1PH}, P_{DC,conv}, P_{DC-load,conv}, P_{sub,uc}^{rated}, P_{sub,bat}^{rated}, P_{DC,uc}^{rated}, P_{PV}^{rated}) \tag{26}$$

When the artificial fish performs the prey behavior, it constantly finds the food consistency in other locations within the field of vision. If the food consistency at the found location is higher than the consistency at the current location, it moves a random distance in that direction, otherwise it will continue to find food consistency at another random location within the field of vision and repeat above steps until the maximum number of *try_number* is reached. If the maximum number of *try_number* is reached and the artificial fish still does not find a location with a higher food consistency than the current location, it will perform random behavior which formula is the same as (24).

Swarm behavior is defined by (27-29):

$$X_C = \frac{\sum_{i=1}^{n_f} X_i}{n_f} \tag{27}$$

$$\frac{Y_C}{n_f} > \delta \cdot Y_k \tag{28}$$

$$X_k^{s+1} = X_k^s + \frac{X_C - X_k^s}{\left\| X_C - X_k^s \right\|_2} \cdot Step \cdot Rand(1) \tag{29}$$

where n_f is the total number of artificial fishes within the field of vision of the current artificial fish *k*. X_C is the center position of these artificial fish positions. Y_C and Y_K denotes the food consistency of center position and current position, respectively. For this paper, the food consistence is R_{total} which is shown in (19). δ presents the crowding factor.

When the artificial fish performs swarm behavior, it first uses (27) to calculate the center position of the fish within the current fish field of vision, and then executes (28). If it meets the conditions of (28), executes (29), otherwise executes prey behavior.

Follow behavior is defined by (36-38):

$$X_{MAX} = \arg\max_X (Y_1, Y_2, ..., Y_{n_f}) \tag{30}$$

$$\frac{Y_{MAX}}{n_f} > \delta \cdot Y_k \tag{31}$$

$$X_k^{s+1} = X_k^s + \frac{X_{MAX} - X_k^s}{\left\| X_{MAX} - X_k^s \right\|_2} \cdot Step \cdot Rand(1) \tag{32}$$

where Y_{MAX} is the maximum food consistency within the field of vision of the current artificial fish k. X_{MAX} the position of the maximum food consistency.

The artificial fish performs follow behavior according to the following steps: First AFSA determines the position of each fish and the corresponding food consistency within current fish's field of vision. Secondly, AFSA uses (30) to find the maximum food consistency and its position of the fish. If maximum food consistency satisfies (31), then execute (32), otherwise execute prey behavior.

For the lower layer optimization, it is implemented by CPLEX solver, and the specific solution method is branch-and-cut method. The details of branch-and-cut method is as follows:

Consider the following MILP problem:

$$u^* = \min\{c^T x + d^T y : x \in R^n, y \in Z^m\} \tag{33}$$

where x is an n-dimensional vector of real variables. y is an m-dimensional vector of integer variables. c^T and d^T are constraint matrices for x and y, respectively.

Solving the MILP problem using the branch-and-cut method generally removes all integer constraints first, so that the MILP problem becomes a linear programming (LP) problem, which is called the linear programming relaxation of the original MILP problem. We can then solve this LP problem, and if the result happens to satisfy all integer constraints, then, luckily, this solution is the optimal solution to the original MILP problem. Otherwise, we need to choose some integer constraint to branch. For the sake of illustration, assuming this variable is y_1, if its value in the LP relaxation problem is 2.4, then we can branch the original LP relaxation problem into two LP problems that respectively satisfy the conditions $y_1 \leqslant 2$ and $y_1 \geqslant 3$. Similarly, in the new branch, if there is no solution that satisfies all integer constraints, we can also choose another integer variable for further branching.

It should be noted that if the optimal solution obtained by a certain branch is smaller than the optimal solution in all current branches, the optimal solution will be updated to the latest optimal solution. And if we find that the lower bound of the optimal solution of a branch is greater than the latest optimal solution, we should cut off the branch, because this branch has no potential to tap the optimal solution. This is where the branch-and-cut method got its name.

For MILP problem of this paper, the real variables vector is shown in (34):

$$\begin{aligned} x = (&P_{sub-grid}, P_{sub,uc,ch}, P_{sub,uc,dis}, P_{sub,bat,ch}, \\ &P_{sub,bat,dis}, P_{DC,uc,ch}, P_{DC,uc,dis}, P_{DC-load}, \\ &P_{10kV\ grid}, P_{sub-grid,\,fed}, E_{sub,uc}, E_{sub,bat}, E_{DC,uc}) \end{aligned} \tag{34}$$

The integer variables vector is shown in (35):

$$y = (b_{sub,uc}, b_{sub,bat}, b_{DC,uc}, b_{sub,grid}) \tag{35}$$

where $b_{sub,uc}$, $b_{sub,bat}$ and $b_{DC,uc}$ respectively present the charge-discharge limit variables of UC on the AC-DC-AC traction substation side, battery on the AC-DC-AC traction substation side and UC on the DC bus of microgrid. Since the energy storage device cannot be charged and discharged at the same time, the above variables are used to limit the state of charge and discharge of the energy storage device. When the above value is 0, the energy storage device is discharged, and when the above value is 1, the energy storage device is charged. $b_{sub,grid}$ is the state limiting variables for the traction substation to obtain electricity from the grid and return electricity to the grid. In the same way, traction substation cannot obtain power from the grid and return power at the same time. Therefore, when the value is 0, the substation obtains power from the grid, and when the value is 1, the substation returns power to the grid.

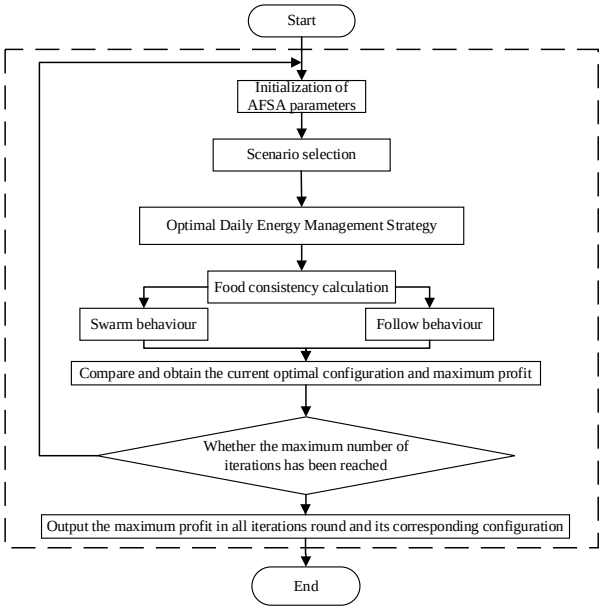

Fig. 3. Flow chart of capacity configuration method.

Based on the above algorithm construction, we can summarize the steps of capacity configuration based on double-layer optimization in this paper as follows:

Step 1 Set the variable range of each variable to be determined and initialize each parameter of the AFSA algorithm.

Step 2 Enter the scenario data, such as the power of traction load, solar irradiance, and the power of 10kV load.

Step 3 Run DEMS and calculate the food consistency at each artificial fish's position according to the DEMS operation results and (19).

Step 4 The swarm behavior and follow behavior are performed for each fish, and the position with the highest food consistency in these two behaviors is selected as the optimal configuration result of the current fish. The number of executions of this step is equal to the total number of fish *N*.

Step 5 The position with the largest food consistency among all fishes is selected as the optimal configuration result for the current round.

Step 6 Determine whether the maximum number of iterations has been reached, and if so, output the maximum profit in all iterations and its corresponding configuration and terminate the program. Otherwise return to **Step 1**.

The specific flow chart of these steps can be shown in Fig. 3.

IV. Case Study

A. Simulation Conditions

To verify the effectiveness and reliability of the proposed capacity configuration method. We designed a scenario of a flexible smart traction power supply interval based on measured data and optimized its capacity configuration based on this scenario.

The departure interval of the train is set as follows: the departure interval between 6:30 and 9:00 is 24 minutes; the departure interval between 9:00 and 16:00 is 12 minutes; the departure interval between 16:00 and 20:00 is 16 minutes; the departure interval between 20:00 and 23:00 is 20 minutes; there is no train for the rest of the time. According to train traction load from Qingzhou to Dezhou in Beijing-Shanghai high-speed railway and the departure interval settings, we could get the traction load power as shown in Fig. 4. The solar irradiation, and 10kV load power which is measured in Fugu substation in Shenshuo Railway are shown in Fig. 4-6, respectively.

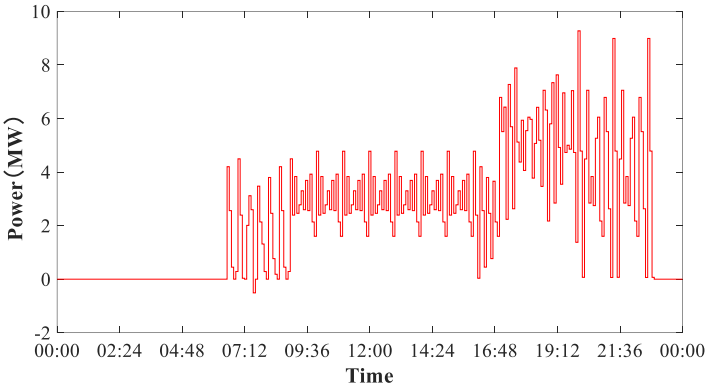

Fig. 4. Schematic diagram of traction load power.

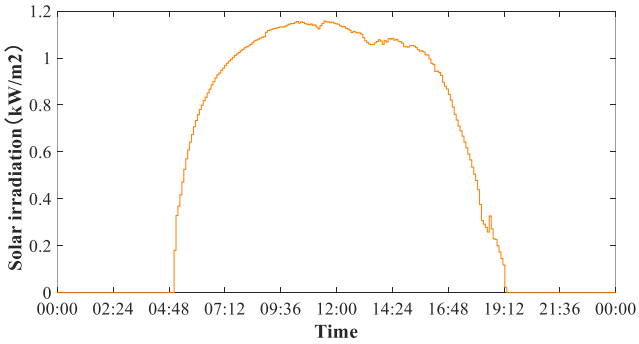

Fig. 5. Schematic diagram of solar irradiation.

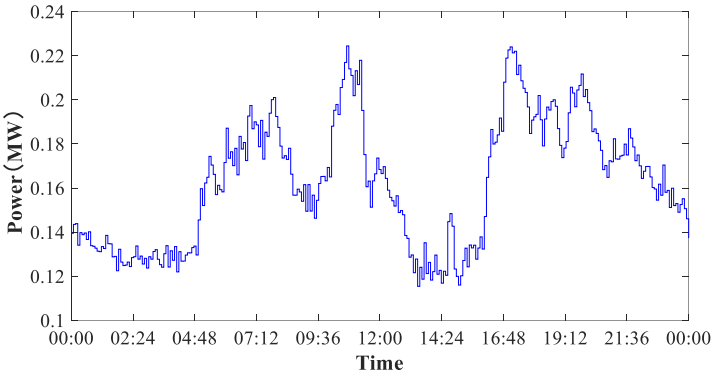

Fig. 6. Schematic diagram of 10kV load power.

The price and life expectancy of each device in FSTPSS are shown in Table I. The overall life expectancy of FSTPSS takes the shortest life expectancy among these devices.

To simplify the analysis of the problem, the same UC or battery modules are combined in series, so the relationship between the power and energy of the UC and the battery is fixed. In fact, if different UC or battery modules are used in series, we just need to separate them into different variables due to the different ratios between power and capacity. For the case study in this paper, the capacity of each MW UC is 0.025MWh, and the capacity of each MW battery is 1.5MWh.

For UC, the charge and discharge efficiency of UC are set to 0.9, the self-discharge coefficient is set to 0.84%/h, and the SOC range is set to 5%~95%. The charge and discharge efficiency of the battery is set to 0.8, the self-discharge coefficient is set to 0.004%/h, and the SOC range is set to 20%~80%.

For PV panels, we also use the same module, so the relationship between its rated power and the area of the PV panel is fixed. In our case study, each MW of PV panels corresponds to 6060 m^2 photovoltaic panel area.

For batteries, UCs and PV panels, the capacity of their converters are equal to their rated power, respectively. And the capacity of the two isolation transformers are respectively equal to the capacity of the converters they connect.

The default parameter settings of AFSA and the range of the capacity configuration of each device that it needs to identify are shown in Table II.

TABLE I
THE PRICE AND LIFE EXPECTANCY OF EACH DEVICE

Device name	Price	life expectancy
UC	¥104,200/MW	20 years
Battery	¥1,975,500/MW	15 years
Converter(3AC/1DC)	¥560,000/MW	25 years
Converter(1DC/1AC)	¥480,000/MW	29 years
Converter(1DC/1DC)	¥83,000/MW	16 years
PV panel	¥485,000/MW	20 years
Isolated transformer	¥30,000/MW	20 years

TABLE II
AFSA PARAMETER SETTING

Parameters	Settings	Parameters	Settings
$P_{sub,converter}^{three\text{-}phase}$	[10,40]MW	P_{PV}^{rated}	[0,2]MW
$P_{sub,converter}^{single\text{-}phase}$	[10,40]MW	δ	0.618
$P_{DC,converter}$	[5,20]MW	*Visual*	0.25
$P_{DC\text{-}load,converter}$	[0,0.5]MW	*Step*	0.1
$P_{sub,uc}^{rated}$	[1,10]MW	*try_number*	2
$P_{sub,bat}^{rated}$	[1,5]MW	*N*	4
$P_{DC,uc}^{rated}$	[1,10]MW	*Maximum iterations*	50

B. Comparison of Benchmark and Optimal Capacity Configuration Results

In order to demonstrate the superiority of the results obtained by the capacity configuration optimization algorithm, we compare it with the results using benchmark parameters. The idea of this capacity parameters is as follows: Considering that PV panels can bring higher benefits, the parameters of PV panels are set to the maximum value, which is 2MW. The converter connecting the 10kV distribution network and the wayside microgrid mainly considers the maximum power of the 10kV distribution network load. Since the maximum power of the 10kV distribution network does not exceed 0.25MW, the converter power is set to 0.25MW. Then, considering that the main function of UC on the microgrid side is to realize the function of peak shaving and valley filling on the microgrid side. Meanwhile, it also needs to accommodate the energy value of the power on the microgrid side within 5 minutes. Since the maximum solar radiation of PV is about 1.2kW/m^2, considering a certain margin, so UC parameter on the microgrid side is set to 8MW. UC power on the AC-DC-AC substation side is set to 10MW, which is higher than the 5-minute peak power of the traction load, but at this time, since the battery is also installed on the AC-DC-AC substation side, it does not need to consider the maximum energy capacity problem. This problem is borne by the battery. The battery on the AC-DC-AC substation side mainly considers the problem of maximum capacity. It mainly considers the regenerative braking power of the train and PV power. Since the sum of its peak power does not exceed 4MW, the battery parameters are set to 4MW. Finally, it is the power of the three-phase converter and the single-phase converter of the AC-DC-AC traction substation, which should be higher than the sum of the charging power and the sum of discharging power of all devices in the system. Therefore, these two parameter values are both set to 30MW.

So, the benchmark parameter is [$P_{sub,conv}^{3PH}$, $P_{sub,conv}^{1PH}$, $P_{DC,conv}$, $P_{DC\text{-}load,conv}$, $P_{sub,uc}^{rated}$, $P_{sub,bat}^{rated}$, $P_{DC,uc}^{rated}$, P_{PV}^{rated}]=[30, 30, 12, 0.25, 10, 2, 8, 2]MW. Based on the benchmark parameters, the maximum benefit in FSTPSS's life expectancy is ¥5.53×10^7.

The final capacity configuration optimization result is [$P_{sub,conv}^{3PH}$, $P_{sub,conv}^{1PH}$, $P_{DC,conv}$, $P_{DC\text{-}load,conv}$, $P_{sub,uc}^{rated}$, $P_{sub,bat}^{rated}$, $P_{DC,uc}^{rated}$, P_{PV}^{rated}]=[10, 10, 11.86, 0.26, 7.59, 4.18, 3.69, 2] MW, and the maximum benefit in FSTPSS's life expectancy is ¥7.94 ×10^7 . Compared with the benchmark, the final converged maximum benefit value has increased by about 43.6%, which verifies the effectiveness of the proposed capacity configuration method. The change of the maximum benefit of AFSA with the number of iterations is shown in Fig. 7. The performance comparison of FSTPSS under the benchmark parameters and the optimal

parameters is summarized in Table III.

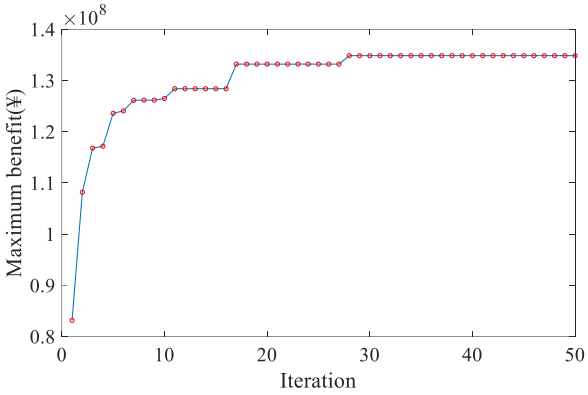

Fig. 7. Schematic diagram of the change of the maximum benefit with the number of iterations

TABLE III
PERFORMANCE Comparison

	Benchmark	Optimal	Growth rate
Equivalent cycle number of sub,uc	16	22.4	28.60%
Equivalent cycle number of sub,bat	1.11	1.22	9.01%
Equivalent cycle number of DC,uc	15.9	18.4	13.60%
Maximum benefit	¥5.53×10^7	¥7.94×10^7	43.60%

C. *Grid Power Optimization Results*

Fig. 8(a) and Fig. 8(b) respectively compare the FSTPSS grid power using the benchmark parameters with the grid power of traditional TPSS and the FSTPSS grid power using the optimal parameters and the grid power of the traditional TPSS. The reduction rate of grid power using two sets of parameters is shown in Table I. From Fig. 8 and Table I, it can be clearly seen that no matter which set of parameters is used, the grid power of FSTPSS can be significantly reduced. However, using the optimal parameters, a greater load reduction rate can be obtained.

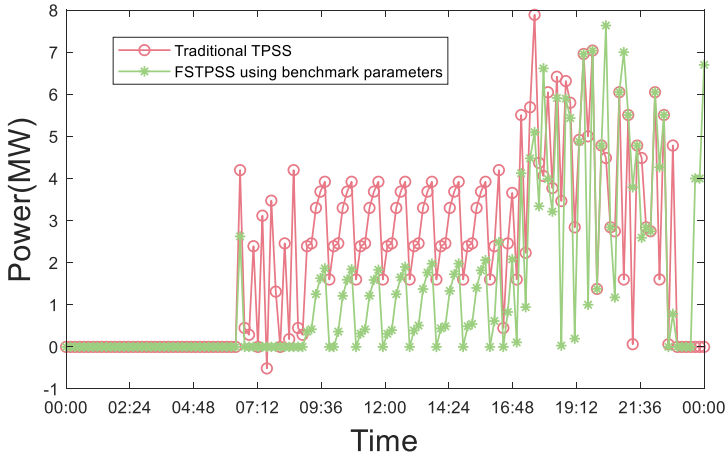

(a)

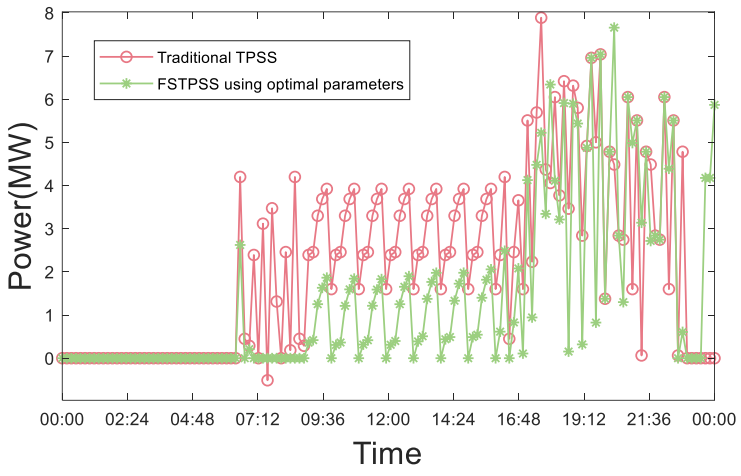

(b)

Fig. 8. Comparison of the grid power of FSTPSS and the grid power of traditional TPSS: (a). FSTPSS using benchmark parameters. (b) FSTPSS using optimal parameters.

TABLE IV
LOAD REDUCTION RATE COMPARISON

	Benchmark	Optimal
Load reduction rate	14.88%	18.33%

In order to further analyze the economic considerations of the capacity configuration method for grid power optimization, we draw a pie chart of the contribution of each factor to economic optimization under the optimal parameters which shown in Fig. 9. Among them, the economic contribution of PV to grid power optimization considers the cost saved by PV supplying power to traction load and 10kV load at each moment. If there is still surplus PV power after supplying power to the traction load and 10kV load, the rest of the energy would be stored in the energy storage device. The energy income stored in the energy storage device is considered as the time-of-use electricity price at the current moment multiplied by the energy storage charge and discharge efficiency. The economic contribution of the train's regenerative braking energy to the grid power optimization only considers the income that store the braking energy in the energy storage device, and the calculation method is the same as that store the rest PV energy in energy storage device. The rest of the grid power optimization benefits are collectively attributed to the benefits obtained by adding energy storage devices and using optimization methods, which are mainly obtained through the price difference of time-of-use electricity prices and peak shaving and valley filling. From the figure, it can see that in addition to the utilization of PV and regenerative braking energy itself to increase the economics of grid power, the reasonable capacity configuration of energy storage devices and energy management process are also important factors to improve the economics.

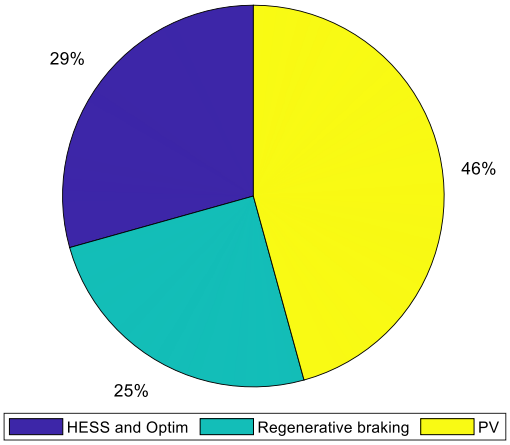

Fig. 9. Composition diagram of economic contribution factors of power grid optimization.

D. Energy Storage Device Optimization Results

The comparison of SOC changes of the energy storage devices with benchmark parameters and optimal parameters are shown in Fig. 10.

From figure, we can see that UC and battery using the optimal parameters has more charge and discharge cycles per day than those using the benchmark parameters. The equivalent charge cycles of UC in substation, battery in substation and UC in microgrid with optimal parameters are 22.4, 1.22 and 18.4, respectively, whereas with benchmark parameters, they are 16.0, 1.11 and 15.9, respectively. These results show that the utilization of UC has become more sufficient. Therefore, the optimal capacity configuration parameters have more charging margin and more efficient energy storage device utilization than the benchmark parameters. The performance comparison of FSTPSS under the benchmark parameters and the optimal parameters is summarized in Table III.

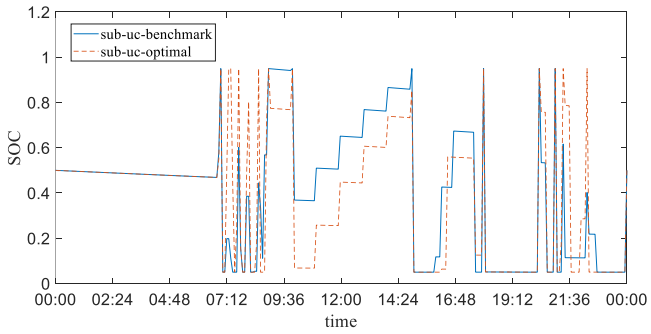

(a)

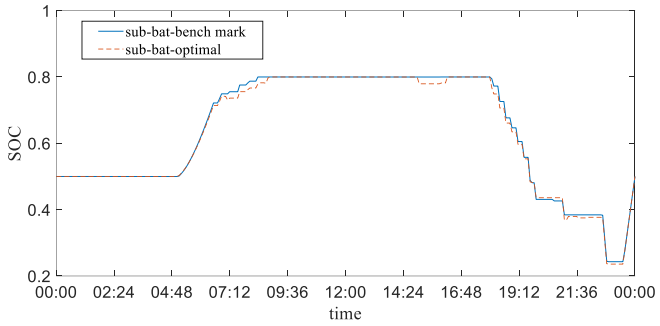

(b)

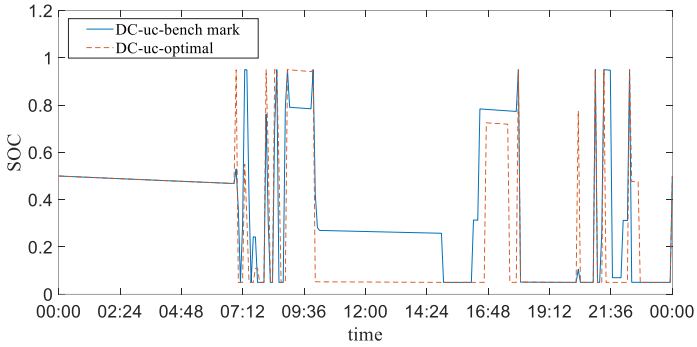

(c)

Fig. 10. Comparison of SOC changes of energy storage devices with benchmark and optimal parameters: (a) UC in AC-DC-AC traction substation. (b) battery in AC-DC-AC traction substation. (c) UC in the DC bus of wayside microgrid.

E. Converter Capacity Utilization results

In order to further verify the efficiency of converter utilization, we also made statistics on the average capacity utilization rate of each converter. The formula for calculating the average capacity utilization rate is as follows:

$$\eta = \frac{P_{i,av}}{P_{i,cap}^{rated}} \cdot 100\% \tag{36}$$

where η is the average capacity utilization rate. $P_{i,av}$ is the average daily power through converter i. $P_{i,cap}{}^{rated}$ is the rated capacity of converter i.

Fig. 11 shows the average utilization rate of capacity of each converter. The capacity utilization rate of the optimal parameters is significantly larger than that of the benchmark parameters. This is because an excessively high capacity vacancy rate is not conducive to the overall economy. Meanwhile, since the traction load has a certain peak load, which is usually three times or more than its average load. Therefore, even with optimal parameters, the capacity utilization of the converter will not exceed 30%.

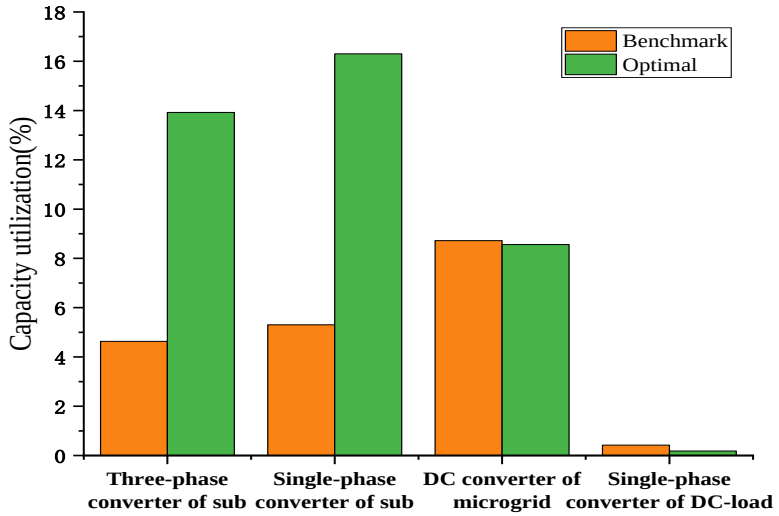

Fig. 11. Capacity utilization of each converter in FSTPSS.

F. Influence analysis of reliability constraints on Capacity Configuration Optimization

Since the traction load has a certain randomness, in order to verify the validity of the reliability constraint under this randomness, we add random fluctuations that obey the $N(0, 2.06)$ distribution to each train load at each moment. N stands for a normal distribution. For a normal distribution $N(\mu, \sigma^2)$, μ represents its mathematical expectation, and σ^2 represents its variance. If the reader wishes to know some details of the randomness of the traction load, please refer to [26].

Fig. 11 shows comparison of reliability of trains passing through the power supply interval before and after the reliability constraints is added to DEMS. When the reliability index is 1, it means that even the grid outage happens, the train can still pass through the power supply interval by relying on the remaining energy of the energy storage devices. When the reliability index is less than 1, it means that the train cannot pass through the power supply interval solely by relying on the remaining energy of the energy storage devices.

From the figure, we can clearly see that the capacity parameters configured after adding reliability constraints can increase the reliability of the train when the grid outage happens. Before adding the reliability constraint, the probability that the train can continue to pass in the event of a grid outage is 0.9965. After the reliability constraint is added, the probability that the train can continue to pass is increased to 0.9120, which verifies the necessity and effectiveness of adding reliability constraints. However, after adding the reliability constraints, the economy of FSTPSS has also suffered a certain loss. Before the reliability constraints are added, the maximum profit of the system is ¥8.48×10^7, and after the reliability constraints are added, the maximum profit of the system is ¥7.94×10^7. This is because the reliability constraints actually require the system to have a larger battery and capacitance capacity, which is unnecessary when grid outage does not happen.

In fact, Equation (7) indicate that there still remaining energy of energy storage devices which can help the train passes through the current power supply interval, but due to the limitation of the rated power of the energy storage devices and the limitation of the minimum SOC of them, the train cannot use them. If we cancel the minimum SOC limitation of the energy storage devices, the train still has a chance to pass the current power supply interval, but it is not recommended in general since operating below the minimum SOC may damage the energy storage devices.

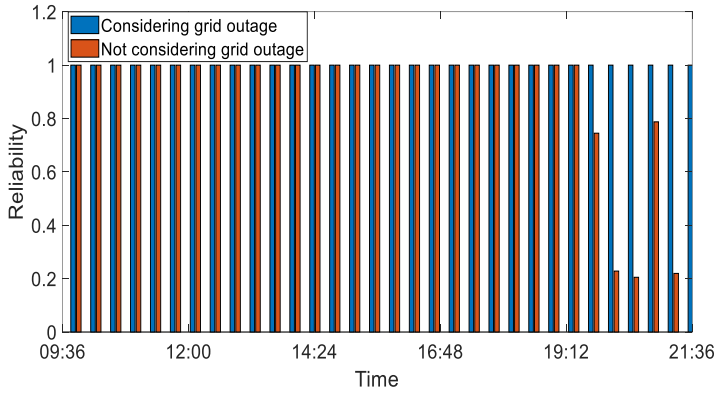

Fig. 11. Comparison of FSTPSS reliability before and after adding reliability constraints.

V. Conclusion

Reasonable capacity configuration is the premise of establishing a FSTPSS that meets the requirements. Based on the limited features and conjectures about the future real FSTPSS, this paper establishes a FSTPSS capacity configuration method, hoping to provide certain recommendations to configure the real FSTPSS in the future. Based on the case study, the following conclusions can be drawn: (1) The system parameters configured by the proposed capacity configuration optimization method can effectively reduce the power obtained by the FSTPSS from the grid and can effectively improve the utilization rate of the battery, UCs and converters. (2) The optimization method of capacity configuration proposed in this paper can significantly improve the overall economy of FSTPSS, so that the investment income of FSTPSS can be significantly improved. (3) If it is necessary to ensure the operational reliability of FSTPSS in the case of grid outage, adding reliability constraints to DEMS allows capacity configuration optimization method to obtain capacity parameters that make the system more reliable. Nevertheless, the economy of FSTPSS will be reduced.

At present, this paper has not yet considered the influence of the randomness of the distributed power supply itself and the energy storage models and TPSS model considered in this paper are not very complex. In the future, if conditions permit, more complex and accurate model of FSTPSS could be studied, and more analysis about impact of the randomness of the distributed power supply on FSTPSS energy management accuracy could be discussed.

REFERENCES

[1] Y. Ying, Q. Liu, M. Wu, and Y. Zhai, “The Flexible Smart Traction Power Supply System and Its Hierarchical Energy Management Strategy,” *IEEE Access*, vol. 9, pp. 64127-64141, 2021.

[2] M. Chen, Z. Cheng, Y. Liu, Y. Cheng and Z. Tian, "Multitime-Scale Optimal Dispatch of Railway FTPSS Based on Model Predictive Control," *IEEE Transactions on Transportation Electrification*, vol. 6, no. 2, pp. 808-820, 2020.

[3] M. Chen, Z. Liang, Z. Cheng, J. Zhao and Z. Tian, "Optimal Scheduling of FTPSS With PV and HESS Considering the Online Degradation of Battery Capacity," *IEEE Transactions on Transportation Electrification*, vol. 8, no. 1, pp. 936-947, 2022

[4] M. Wang, S. Tan, C. Lee, and S. Y. Hui, "A Configuration of Storage System for DC Microgrids," *IEEE Transactions on Power Electronics*, vol. 33, no. 5, pp. 3722-3733, 2018.

[5] N. Yahya Soltani and A. Nasiri, "Chance-Constrained Optimization of Energy Storage Capacity for Microgrids," *IEEE Transactions on Smart Grid*, vol. 11, no. 4, pp. 2760-2770, 2020.

[6] M. Petrelli, D. Fioriti, A. Berizzi, and D. Poli, "Multi-Year Planning of a Rural Microgrid Considering Storage Degradation," *IEEE Transactions on Power Systems*, vol. 36, no. 2, pp. 1459-1469, 2021.

[7] F. Fang, Z. Zhu, S. Jin, and S. Hu, "Two-Layer Game Theoretic Microgrid Capacity Optimization Considering Uncertainty of Renewable Energy," *IEEE Systems Journal*, vol. 15, no. 3, pp. 4260-4271, 2021.

[8] P. Xie, Z. Cai, P. Liu, X. Li, Y. Zhang, and D. Xu, "Microgrid System Energy Storage Capacity Optimization Considering Multiple Time Scale Uncertainty Coupling," *IEEE Transactions on Smart Grid*, vol. 10, no. 5, pp. 5234-5245, 2019.

[9] S. Chalil Madathil et al., "Resilient Off-Grid Microgrids: Capacity Planning and N-1 Security," *IEEE Transactions on Smart Grid*, vol. 9, no. 6, pp. 6511-6521, 2018.

[10] C. C. Thompson, P. E. Konstantinos Oikonomou, A. H. Etemadi, and V. J. Sorger, "Optimization of Data Center Battery Storage Investments for Microgrid Cost Savings, Emissions Reduction, and Reliability Enhancement," *IEEE Transactions on Industry Applications*, vol. 52, no. 3, pp. 2053-2060, 2016.

[11] S. A. Arefifar and Y. A.-R. I. Mohamed, "DG Mix, Reactive Sources and Energy Storage Units for Optimizing Microgrid Reliability and Supply Security," *IEEE Transactions on Smart Grid*, vol. 5, no. 4, pp. 1835-1844, 2014.

[12] A. Mohammad-Alikhani, A. Mahmoudi, R. Khezri, and S. Kahourzade, "Multiobjective Optimization of System Configuration and Component Capacity in an AC Minigrid Hybrid Power System," *IEEE Transactions on Industry Applications*, vol. 58, no. 3, pp. 4158-4170, 2022.

[13] W. Huang, X. Zhang, K. Li, N. Zhang, G. Strbac, and C. Kang, "Resilience Oriented Planning of Urban Multi-Energy Systems With Generalized Energy Storage Sources," *IEEE Transactions on Power Systems*, vol. 37, no. 4, pp. 2906-2918, 2022.

[14] S. Y. Lee, Y. G. Jin, and Y. T. Yoon, "Determining the Optimal Reserve Capacity in a Microgrid With Islanded Operation," *IEEE Transactions on Power Systems*, vol. 31, no. 2, pp. 1369-1376, 2016.

[15] J. Chen, H. Hu, Y. Ge, K. Wang, and Z. y. He, "Techno-Economic Model-Based Capacity Design Approach for Railway Power Conditioner-Based Energy Storage System," *IEEE Transactions on Industrial Electronics*, vol. 69, no. 5, pp. 4730-4741, 2022.

[16] P. Luo *et al.*, "Multi-Application Strategy Based on Railway Static Power Conditioner With Energy Storage System," *IEEE Transactions on Intelligent Transportation Systems*, vol. 22, no. 4, pp. 2140-2152, 2021.

[17] S. D'Arco, L. Piegari, and P. Tricoli, "Comparative Analysis of Topologies to Integrate Photovoltaic Sources in the Feeder Stations of AC Railways," *IEEE Transactions on Transportation Electrification*, vol. 4, no. 4, pp. 951-960, 2018.

[18] F. Zhu, Z. Yang, Z. Zhao, and F. Lin, "Two-Stage Synthetic Optimization of Supercapacitor-Based Energy Storage Systems, Traction Power Parameters and Train Operation in Urban Rail Transit," *IEEE Transactions on Vehicular Technology*, vol. 70, no. 9, pp. 8590-8605, 2021.

[19] A. Zahedmanesh, K. M. Muttaqi, and D. Sutanto, "A Sequential Decision-Making Process for Optimal Technoeconomic Operation of a Grid-Connected Electrical Traction Substation Integrated With Solar PV and BESS," *IEEE Transactions on Industrial Electronics*, vol. 68, no. 2, pp. 1353-1364, 2021.

[20] X. Zhou, X. Yu, Y. Zhang, Y. Luo, and X. Peng, "Trajectory Planning and Tracking Strategy Applied to an Unmanned Ground Vehicle in the Presence of Obstacles," *IEEE Transactions on Automation Science and Engineering*, vol. 18, no. 4, pp. 1575-1589, 2021.

[21] J. Tang, G. Liu, and Q. Pan, "A Review on Representative Swarm Intelligence Algorithms for Solving Optimization Problems: Applications and Trends," *IEEE/CAA Journal of Automatica Sinica*, vol. 8, no. 10, pp. 1627-1643, 2021.

[22] X. Lei, X. Yang, and F. X. Wu, "Artificial Fish Swarm Optimization Based Method to Identify Essential Proteins," *IEEE/ACM Trans Comput Biol Bioinform*, vol. 17, no. 2, pp. 495-505, Mar-Apr 2020.

[23] IBM ILOG CPLEX Optimization StudioV12.10.0 documentation [Online] Available: https://www.ibm.com/support/knowledgecenter/zh/SSSA5P_12.10.0/COS_KC_home.html.

[24] M. Barros and M. Casquilho, "Linear Programming with CPLEX: An Illustrative Application Over the Internet CPLEX in Fortran 90," 2019 14th Iberian Conference on Information Systems and Technologies (CISTI), Coimbra, Portugal, 2019, pp. 1-6.

[25] L. Sun, W. Liu, B. Xu and T. Chai, "The scheduling of steel-making and continuous casting process using branch and cut method via CPLEX optimization," 5th International Conference on Computer Sciences and Convergence Information Technology, Seoul, Korea (South), 2010, pp. 716-721.

[26] S. Yang, K. Song, and G. Zhu, "Stochastic Process and Simulation of Traction Load for High Speed Railways," *IEEE Access*, vol. 7, pp. 76049-76060, 2019.